Automated intracranial vessel labeling with learning boosted by vessel connectivity, radii and spatial context

Jannik Sobisch JANNIK.SOBISCH@GMAIL.COM
Žiga Bizjak ZIGA.BIZJAK@FE.UNI-LJ.SI
Aichi Chien AICHI@UCLA.EDU
Žiga Špiclin ZIGA.SPICLIN@FE.UNI-LJ.SI
Laboratory of Imaging Technologies, Faculty of electrical engineering, University of Ljubljana.
Dept. of Radiological Sciences, David Geffen School of Medicine at UCLA

Editor: Editor's name

Abstract

Cerebrovascular diseases are among the world's top causes of death and their screening and diagnosis rely on angiographic imaging. We focused on automated anatomical labeling of cerebral arteries that enables their cross-sectional quantification and inter-subject comparisons and thereby identification of geometric risk factors correlated to the cerebrovascular diseases. We used 152 cerebral TOF-MRA angiograms from three publicly available datasets and manually created reference labeling using Slicer3D. We extracted centerlines from nnU-net based segmentations using VesselVio and labeled them according to the reference labeling. Vessel centerline coordinates, in combination with additional vessel connectivity, radius and spatial context features were used for training seven distinct PointNet++ models. Model trained solely on the vessel centerline coordinates resulted in ACC of 0.93 and across-labels average TPR was 0.88. Including vessel radius significantly improved ACC to 0.95, and average TPR to 0.91. Finally, focusing spatial context to the Circle of Willis are resulted in best ACC of 0.96 and best average TPR of 0.93. Hence, using vessel radius and spatial context greatly improved vessel labeling, with the attained perfomance opening the avenue for clinical applications of intracranial vessel labeling.

Keywords: Angiograms, MRA, Segmentation, Vessel Centerline, Geometric Learning

1. Introduction

Cerebrovascular diseases are the second most common cause of death; therefore, their early diagnosis and treatment are crucial for preventing adverse health events or even death. In this work, we focused on anatomical labeling of cerebral arteries that enables their cross-sectional quantification and inter-subject comparisons, e.g. healthy versus pathological. Such comparisons are the basis to identify geometric risk factors correlated to the cerebrovascular diseases. Labels provide anatomical localization of features relevant to disease, and support the interpretation of findings. Automation of anatomical labeling is an important step towards higher accuracy, reliability and efficiency of the labeling process and is needed for its practical implementation.

Labeling the Circle of Willis (CoW) is a challenging task due to the variable and complex topology of intracranial vessels. Manual labeling, which relies on visual interpretation of radiologist, is monotonous and time-consuming work (Pugliese et al., 2009), which both introduces deviations into the results and delays further processing (de Giessen et al.,

© 2022 J. Sobisch, Ž. Bizjak, A. Chien & Ž. Špiclin.

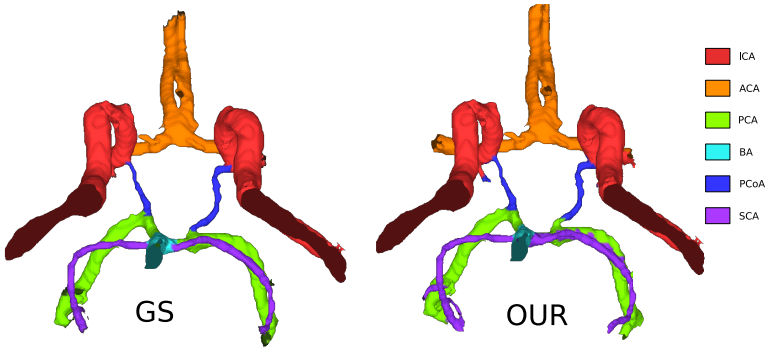

Figure 1: Color-coded vessel labeling superimposed on intracranial vessel wall surface obtained by manual labeling (*left*) and using our best automated approach (*right*).

2015). Automatic labeling is therefore necessary to limit human error and speed up analysis. Smaller vessels, such as the PCoA (Posterior Communicating Artery), represent a tiny fraction of the entire image and their segmentation and labeling entails annotation of only a few voxels, which makes the automation of this process rather difficult.

Most previous studies involved a small number of subjects; one of the causes might be the lengthy process of manually labeling each subject. For instance, Uchiyama et al. (2006) were among the first to address the issue of automatic labeling and used 10 cases and achieved a TPR of 92.5%. Bogunović et al. (2011) proposed a method to annotate five bifurcations in the front (anterior) part of the CoW. While the annotation process was automatic, it was applied on the vessel centerlines obtained using a semi-automatic process. The method was evaluated on vessel images of 30 patients and achieved 90% correct vessel labeling. Two years later the same authors used the whole CoW and on the same dataset achieved a TPR of 95%. Robben et al. (2016) introduced an innovative simultaneous decomposition and labeling of the CoW, allowing them to take advantage of additional raw image information when solving the problem. On 50 MRA images they accurately labeled 95% of all bifurcations. A machine learning approach was proposed by Wang et al. (2017). On 50 MRA images of the cerebral vessels, they annotated the bifurcations with 99% accuracy. Yao et al. (2020) labeled 13 head and neck vessels using a graph convolutional network based pointcloud approach, obtaining a average DSC of 85.9% labeling 4 major head vessels across 72 CT images.

To the best of our knowledge, previous studies tested and refined their vessel labeling methods using no more than 72 images and the authors did not attempt to utilize publicly accessible angiographic datasets, such as the IXI dataset (IXI), which would form the basis for objective cross-comparisons of the labeling results. Furthermore, the whole process of labeling was generally not fully automated as the vessel segmentation and centerline extraction involved manual or semi-automated approaches, or were assumed given a priori.

In this paper, we propose an automated approach to vessel labeling from raw TOF-MRA angiograms obtained from three publicly available datasets. The approach was evaluated on 152 MRA scans and entailed automatic vessel segmentation and centerline extraction

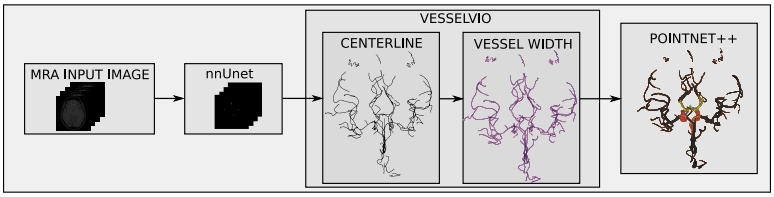

Figure 2: Angiographic scans are first segmented into vessel/background using nnU-Net, then VesselVio (Bumgarner and Nelson, 2022) is used to extract the vessel centerlines, connecting edges and vessel radii, and, finally, this information is applied in the PointNet++ model to predict the vessel labels.

and learning-based labeling of the vessel centerlines. The applied classifier was a modified PointNet++ model using additional features obtained through the vessel centerline extraction. In an ablation-type study we tested seven models, two without and four with different combinations of the additional vessel features, and one model trained only on the CoW area. All models were objectively and comparatively evaluated on the large public and manually labeled dataset using a common evaluation protocol.

2. Methodology

We propose a fully automated method for vessel segmentation, centerline extraction, and vessel labeling, focusing on the intracranial vessels of the CoW as depicted in angiographic scans. Figure 2 presents a basic flowchart of our method.

2.1. Vessel segmentation

For segmenting the vessels from raw angiograms we used nnU-Net (Isensee et al., 2021), a self-adapting framework for U-Net based biomedical image segmentation. The preprocessing of the raw angiograms was fully automated using the nnU-Net pipeline. The annotations for model training consisted of an intracranial vasculature mask, which was manually segmented from the angiograms by an experienced rater using Slicer3D (Pieper et al., 2004).

Next, the binary segmentations were converted to surface models and visualized. Using surface annotation tools in Slicer3D, the vessels were labeled as: ICA (Internal carotoid artery), ACA (Anterior cerebral artery), PCA (Posterior cerebral artery), PCoA (Posterior communicating artery), BA (Basilar artery), SCA (Superior cerebral artery) and OV (other non-CoW vessels).

The obtained segmentations and label maps were reviewed and approved by a neuroradiologist with more than 10 years of experience. The manual labels thus served as a reliable benchmark for the training and validation of our models.

2.2. Centerline extraction

From vessel segmentations we extracted the vessel centerline points, a list of edges interconnecting the centerline points, and the vessel radius associated with each centerline using

VesselVio (Bumgarner and Nelson, 2022). When constructing an undirected graph, VesselVio first determines the vessel centerline using a thinning algorithm (Lee et al., 1994) and then connects the centerline points using a 26-connectivity neighborhood operator. Next, the obtained graph is filtered using a variety of methods to remove erroneously extracted segments and spuriously overlabeled branchpoints. We increased the threshold at which the filtering process begins to eliminate very big branchpoint clusters because the original VesselVio filtering algorithm appeared to overfilter some segments, leaving gaps between otherwise neighboring centerlines.

For training and evaluation purposes the manual labels annotated on the vessel surface were propagated to the vessel centerlines.

2.3. Label prediction

The vessel centerlines and associated vessel labels, list of interconnected neighboring centerlines, and vessel radius were applied to train a model for the classification of centerline label. We used the centerline point connections based on the extracted edgelists, which encoded pairs of interconnected centerline points. This information was used to augment the input to the models, namely by including the coordinates of the two interconnected centerline points and the mean vessel radius at those points.

The label prediction models were trained through resampling the centerlines and associated features. To improve the capability to represent smaller features present in the vessel centerlines, the graph of the extracted labeled centerline points was divided into smaller partially overlapping graphs to be used for model training. Namely, following the selection of a seed point at a random centerline point in the vessel centerline graph, an unstructured point cloud was created by sampling 1000 points based on their Euclidean distance from the seed point. By repeated sampling of the vessel centerline graph we obtained 70 partially overlapping vessel centerline subgraphs for each input angiogram.

To test the contribution of each input feature, an ablation-type study was performed by progressively including features, and training and evaluating several models.

2.3.1. Classifier

To perform vessel labeling, we used PointNet++ as vessel centerline classification model (Qi et al., 2017b). The basic PointNet (Qi et al., 2017a) model inputs unstructured point cloud data and identifies two mapping functions, i.e. $h : \mathbb{R}^N \rightarrow \mathbb{R}^K$ and $g : \mathbb{R}^K \times \mathbb{R}^K \times \mathbb{R}^K\} \rightarrow \mathbb{R}$, which together approximate a general function $f(\{x_1, \ldots, x_n\}) \approx g(h(x_1), \ldots, h(h(x_n)))$. PointNet uses the functions h() and g() on N input points in order to apply the input and feature transformations, and then aggregates the features using maximum pooling. This reduces the input shape to a small and constant number of important keypoints.

PointNet++ builds upon the PointNet model, adding density adaptive layers and a hierarchical abstraction of regions instead of a single max pooling operation. We used two different PointNet++ approaches: Single- and Multi-Scale Grouping (SSG and MSG, resp.). Compared to SSG, the MSG extracts *multi-scale* patterns by applying *multiple* PointNet models after the grouping layers, with input point set size being $N' \times (d + C)$ and output set size $N' \times K \times (d + C)$, thus forming multi scale features.

2.3.2. Aggregation of predictions

In similar manner as the training of the model,in the prediction phase, each vessel centerline graphs was sampled to obtain 70 local overlapping subgraphs of 1000 points, and each subgraph was independently labeled using the trained model. Each centerline point was thus labeled multiple times and its final label was chosen by applying majority voting rule.

3. Evaluation

In this work we propose seven different vessel centerline label prediction models and evaluate their performance on the vessel centerline graphs obtained from automatic segmentation of 152 MRA images. All the models, including nnU-net for vessel segmentation and PointNet++ for label prediction, were trained and tested using 4-fold cross validation. Each fold used 114 MRA images for training and 38 for validating. Out of 114 images, 86 were used for training and 28 for testing and fine-tuning the models in training phase.

3.1. Dataset

The 152 MRAs were obtained from three different publicly available datasets, i.e. IXI (IXI), TubeTK (Bullitt et al., 2005) and ADAM dataset (Timmins et al., 2021). From the IXI dataset we took 80 subjects (43 women and 37 men) aged between 21 and 75 years, with the MRAs acquired using three different scanners: Philips 3T, Philips 1.5T and GE 1.5T. From the TubeTK dataset we used 29 subjects (19 women and 10 men) between 20 and 49 years, with all MRAs acquired by a Siemens Allegra 3T. From the ADAM dataset we took 43 subjects (29 women and 14 men) aged between 19 and 61 years, whereas the MRAs were acquired on different Philips scanners with field strength of either 1, 1.5 or 3T. Combining MRA scans acquired across different scanner vendors, protocols and field strengths enabled us to rigorously test the accuracy and robustness of the methods and thus assess their fit for clinical application.

3.2. Experiment

We used two variants of PointNet++, i.e. SSG and MSG, in combination with input centerline point coordinates and additional features. Namely, SSG_Base input the extracted centerline point coordinates (input size: $N \times 3$), SSG_Rad additionally input vessel radius associated with each centerline point (input size: $N \times 4$), while SSG_CR used the pairs of point connections and their corresponding vessel radius (input size: $N \times 7$). With the same respective inputs we also tested the PointNet++ MSG, denoted as MSG_Base, MSG_Rad and MSG_CR.

Finally, we used the best-performing of the aforementioned six models and trained the model on vessel centerline graphs cropped to the CoW region (MSG_ROI). Furthermore, we trained a separate model for binary labeling of the CoW dubbed MSG_CoW in order to demonstrate that the area of the CoW can be detected automatically; consequently, the MSG_ROI model application is fully automatic.

For training all the models we used the Adam optimizer with the learning rate set to 0.001, the decay rate to 0.5, and the decay step to 20.

Table 1: Vessel labeling performance across all seven tested prediction models. Values in **bold** highlight the best results per performance metric, separately for global models and the model limited to the CoW area.

Model	ACC	avgDSC	avgTPR
SSG_Base	0.930	0.754	0.884
SSG_Rad	0.933	0.778	0.894
SSG_CR	0.940	0.787	0.870
MSG_Base	0.943	0.782	0.887
MSG_Rad	**0.947**	**0.804**	**0.904**
MSG_CR	0.946	0.800	0.884
MSG_ROI	**0.957**	**0.913**	**0.932**

Labeling performance was evaluated by calculating the overall accuracy (ACC), true positive rate (TPR) and Dice similarity coefficient (DSC). In order to additionally penalize incorrect predictions on the smaller vessels, the TPR and DSC were computed for each of the n vessel segments individually, added up and divided by vessels present in the case:

$$\text{avgTPR} = \sum_{i=1}^{n} \frac{\text{TPR}_\text{i}}{n}\,, \qquad \text{avgDSC} = \sum_{i=1}^{n} \frac{\text{DSC}_\text{i}}{n}\,. \tag{1}$$

4. Results

Average DSC and TPR calculated across test cases in all four folds are reported in Table 1. The PointNet++ SSG-based models resulted in overall lower performance compared to the MSG-based models. The PointNet++ model without additional features (e.g. SSG_Base) achieved lowest score of average DSC 0.754 and TPR of 0.884, while SSG_Rad and SSG_CR slightly improved the results with average DSCs of 0.778 and 0.787, respectively.

The MSG_Base achieved the average DSC of 0.782, while the MSG_Rad and MSG_CR achieved comparable average DSC of 0.804 and 0.800, respectively, but the MSG_Rad achieved better average TPR (0.904 compared to 0.884 of the MSG_CR). In the final experiment, the MSG_Rad model was used to train MSG_ROI model in the area as identified by the MSG_CoW; the MSG_ROI achieved the overall best results (average DSC of 0.913). All results are summarized in Table 1. As a sidenote, the supporting model MSG_CoW that labeled the CoW versus other vessels achieved a TPR of 0.996 for the CoW vessels and an overall ACC of 0.968.

We further analyzed the two best performing models based on each vessel label, i.e. MSG_ROI and MSG_Rad. The improvements by MSG_ROI were especially evident in smaller vessels such as PCoA, where the DSC of MSG_ROI (0.757) was much higher than the DSC of MSG_Rad (0.570). For larger vessels, such as ICA, the DSC improved slightly from 0.921 to 0.979. The per vessel label results are presented in Table 2. A set of boxplots that compare the TPR of the models for each vessel are shown in Figure 3. Even though the performance increase of MSG_ROI shown might not be as apparent for the bigger vessels

Table 2: Performance comparison between the two best performing models MSG_ROI and MSG_Rad. For each vessel label the TPR, DSC and Precision are reported. Values in **bold** denote the best results per each vessel label.

	Model	ICA	ACA	PCA	PCoA	BA	SCA	OV
TPR	MSG_Rad	0.972	0.942	0.902	0.761	0.871	0.899	0.948
	MSG_ROI	**0.981**	**0.979**	**0.959**	**0.813**	**0.888**	**0.946**	–
DSC	MSG_Rad	0.921	0.821	0.772	0.570	0.822	0.731	0.966
	MSG_ROI	**0.979**	**0.970**	**0.946**	**0.757**	**0.898**	**0.879**	–
Precision	MSG_Rad	0.881	0.731	0.692	0.585	0.820	0.634	0.989
	MSG_ROI	**0.978**	**0.965**	**0.937**	**0.814**	**0.925**	**0.884**	–

such as the ICA, ACA or PCA, we can still observe an increase of median TPR from 0.987 to 0.991, 0.984 to 0.993 and 0.944 to 0.986 respectively, as well as a lower amount of outliers in the lower quartiles, further solidifying the improvement offered by MSG_ROI.

5. Discussion

A novel fully automated approach that uses the nnU-net vessel segmentation and upon extracted vessel centerlines so as to label the six most relevant CoW vessel and differentiate them from the distal non-CoW vessels. The CoW is a crucial area of the cerebrovascular system that is vulnerable to a number of diseases, including intracranial aneurysms, which usually develop there (Brisman et al., 2006). The reliable automatic labeling algorithm proposed in this paper opens up the possibility to conduct further research into the relationship between size and presence of specific vessels or the development and rupture of intracranial aneurysms.

We tested six different models on the full intracranial vessel centerline graph to fully evaluate the contribution of each parameter to the labeling quality. The best average TPR

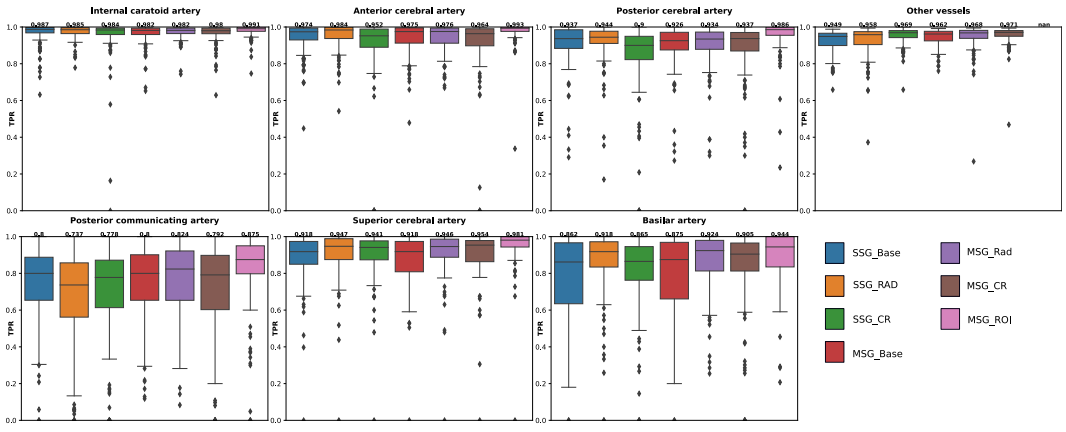

Figure 3: Boxplots of TPR across all vessel labels and all seven tested models.

of 0.904 was achieved by model MSG_Rad; however, the average TPRs of the other five models were fairly close (see Table 1. For example, the boxplots in Figure 3 show a distinct difference between the models abilities to label the PCoA, SCA, and BA. On bigger vessels like the ICA, ACA, and PCA, the differences are minor.

As we are most interested in the CoW region, we trained the final MSG_ROI model exclusively in this area, where the area was first automatically determined by the MSG_CoW model and then the data labeling model was trained and applied. The general area of the CoW was detected by the MSG_CoW, which achieved a TPR of 0.996 on CoW vessels and overall ACC of 0.968. The MSG_ROI model was based on the top-performing model from the first six experiments MSG_Rad, and yielded state of the art average TPR of 0.932 and also state of the art ACC (0.957) and average DSC (0.911). It is clear that by focusing on the area of interest, the model labeling capabilities were greatly enhanced.

Figure 3 further demonstrates that MSG_ROI model outperforms every other model on across all vessels labels while offering a more robust performance as indicated the lower interquartile range. Comparing models MSG_Rad and MSG_ROI revealed significant improvement of DSC for the PCoA (from 0.57 to 0.76), a small vessel which is typically overlooked or mislabeled due to its small size and thickness. In our evaluation we used class-averaged TPR and DSC, which penalizes cases equally for each vessel label, regardless of the vessel size. In this manner, the impact of smaller vessels (like PCoA) on the final score is equal to that of larger vessels (such as ICA). Current state-of-the-art approaches typically only report overall true positive rate or accuracy, so if a small vessel is poorly or even not identified, the overall score is not substantially affected. Their contribution to the final score is further diminished by the fact that PCoA vessels are not included in all cases (Hartkamp and van der Grond, 2000). Our result for cases with and without PCoA vessel can be seen in Figure 4.

The proposed method is heavily dependent on vessel centerline extraction using the VesselVio program, which occasionally produces sub standard results. As shown on the right side of Figure 4, this may lead to poor labeling. Our long-term goal is to decrease the number of incorrectly labeled vessels, which we think can be done by enhancing the cerebral vessel centerline extraction algorithm with a focus on CoW.

In conclusion, a novel automated CoW labeling approach was proposed using the vessel centerline coordinates, connectivity and radii, extracted from segmented angiograpms, as input to a PointNet++ model, achieving average TPR of 0.904 using vessel centerline graph, or 0.931 if the spatial context including CoW area vessel subgraphs was used.

Acknowledgments

Part of MR brain images from healthy volunteers used in this paper were collected and made available by the CASILab at The University of North Carolina at Chapel Hill and were distributed by the MIDAS Data Server at Kitware, Inc. This study was supported by the Slovenian Research Agency (Core Research Grant No. P2-0232 and Research Grants Nos. J2-2500 and J2-3059) and in part by NIH R01HL152270.

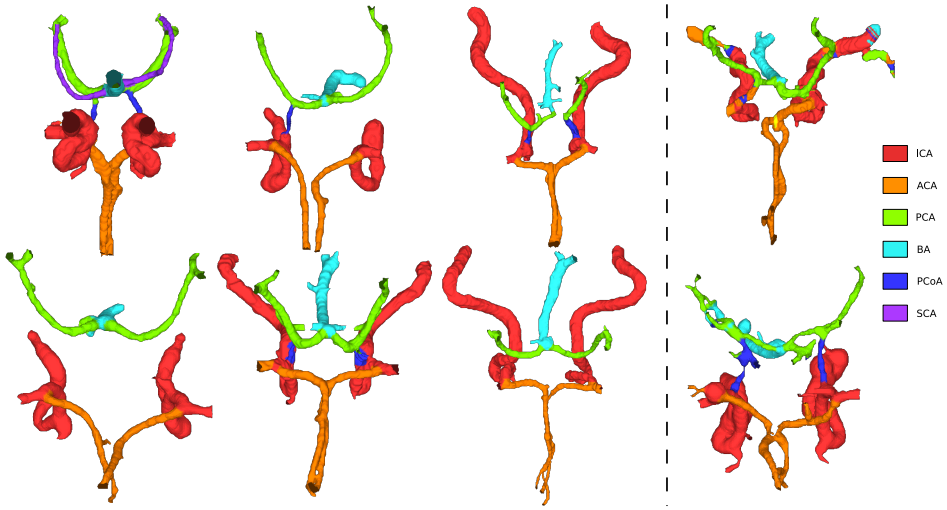

Figure 4: Comparison of good (*left*) and bad (*right*) vessel label prediction results of our approach, visualized on rendered meshes.

References

IXI Dataset – Brain Development. URL https://brain-development.org/ixi-dataset/.

Hrvoje Bogunović, José María Pozo, Rubén Cárdenes, and Alejandro F. Frangi. Anatomical Labeling of the Anterior Circulation of the Circle of Willis Using Maximum a Posteriori Classification. In Gabor Fichtinger, Anne Martel, and Terry Peters, editors, *Medical Image Computing and Computer-Assisted Intervention – MICCAI 2011*, Lecture Notes in Computer Science, pages 330–337, Berlin, Heidelberg, 2011. Springer. ISBN 978-3-642-23626-6. doi: 10.1007/978-3-642-23626-6_41.

Jonathan L. Brisman, Joon K. Song, and David W. Newell. Cerebral aneurysms. *N Engl J Med*, 355(9):928–939, August 2006. ISSN 1533-4406. doi: 10.1056/NEJMra052760.

Elizabeth Bullitt, Donglin Zeng, Guido Gerig, Stephen Aylward, Sarang Joshi, J Keith Smith, Weili Lin, and Matthew G Ewend. Vessel tortuosity and brain tumor malignancy: a blinded study1. *Academic radiology*, 12(10):1232–1240, 2005.

Jacob R. Bumgarner and Randy J. Nelson. Open-source analysis and visualization of segmented vasculature datasets with vesselvio. *Cell Reports Methods*, 2(4):100189, 2022. ISSN 2667-2375. doi: https://doi.org/10.1016/j.crmeth.2022.100189. URL https://www.sciencedirect.com/science/article/pii/S2667237522000443.

Martijn Van de Giessen, Jasper P. Janssen, Patrick A. Brouwer, Johan H. C. Reiber, Boudewijn P. F. Lelieveldt, and Jouke Dijkstra. Probabilistic atlas based labeling of

the cerebral vessel tree. In Sébastien Ourselin and Martin A. Styner, editors, *SPIE Proceedings*. SPIE, March 2015. doi: 10.1117/12.2081604. URL https://doi.org/10.1117/12.2081604.

M.J. Hartkamp and Jeroen van der Grond. Investigation of the Circle of Willis using MR angiography. *MedicaMundi*, 44:20–27, January 2000.

Fabian Isensee, Paul F Jaeger, Simon AA Kohl, Jens Petersen, and Klaus H Maier-Hein. nnu-net: a self-configuring method for deep learning-based biomedical image segmentation. *Nature methods*, 18(2):203–211, 2021.

Ta-Chih Lee, Rangasami L Kashyap, and Chong-Nam Chu. Building skeleton models via 3-d medial surface axis thinning algorithms. *CVGIP: Graphical Models and Image Processing*, 56(6):462–478, 1994.

Steve Pieper, Michael Halle, and Ron Kikinis. 3d slicer. In *2004 2nd IEEE international symposium on biomedical imaging: nano to macro (IEEE Cat No. 04EX821)*, pages 632–635. IEEE, 2004.

Francesca Pugliese, M. G. Myriam Hunink, Katarzyna Gruszczynska, Filippo Alberghina, Roberto Malagó, Niels van Pelt, Nico R. Mollet, Filippo Cademartiri, Annick C. Weustink, Willem B. Meijboom, Cilia L. M. Witteman, Pim J. de Feyter, and Gabriel P. Krestin. Learning curve for coronary CT angiography: What constitutes sufficient training? *Radiology*, 251(2):359–368, May 2009. doi: 10.1148/radiol.2512080384. URL https://doi.org/10.1148/radiol.2512080384.

Charles R Qi, Hao Su, Kaichun Mo, and Leonidas J Guibas. Pointnet: Deep learning on point sets for 3d classification and segmentation. In *Proceedings of the IEEE Conference on Computer Vision and Pattern Recognition*, pages 652–660, 2017a.

Charles Ruizhongtai Qi, Li Yi, Hao Su, and Leonidas J Guibas. PointNet++: Deep Hierarchical Feature Learning on Point Sets in a Metric Space. In I. Guyon, U. Von Luxburg, S. Bengio, H. Wallach, R. Fergus, S. Vishwanathan, and R. Garnett, editors, *Advances in Neural Information Processing Systems*, volume 30. Curran Associates, Inc., 2017b. URL https://proceedings.neurips.cc/paper/2017/file/d8bf84be3800d12f74d8b05e9b89836f-Paper.pdf.

David Robben, Engin Türetken, Stefan Sunaert, Vincent Thijs, Guy Wilms, Pascal Fua, Frederik Maes, and Paul Suetens. Simultaneous segmentation and anatomical labeling of the cerebral vasculature. *Med Image Anal*, 32:201–215, August 2016. ISSN 1361-8423. doi: 10.1016/j.media.2016.03.006.

Kimberley M Timmins, Irene C van der Schaaf, Edwin Bennink, Ynte M Ruigrok, Xingle An, Michael Baumgartner, Pascal Bourdon, Riccardo De Feo, Tommaso Di Noto, Florian Dubost, et al. Comparing methods of detecting and segmenting unruptured intracranial aneurysms on tof-mras: The adam challenge. *Neuroimage*, 238:118216, 2021.

Yoshikazu Uchiyama, Masashi Yamauchi, Hiromichi Ando, Ryujiro Yokoyama, Takeshi Hara, Hiroshi Fujita, Toru Iwama, and Hiroaki Hoshi. Automated classification of

cerebral arteries in MRA images and its application to maximum intensity projection. *Conf Proc IEEE Eng Med Biol Soc*, 2006:4865–4868, 2006. ISSN 1557-170X. doi: 10.1109/IEMBS.2006.260438.

Xingce Wang, Yue Liu, Zhongke Wu, Xiao Mou, Mingquan Zhou, Miguel Ángel González Ballester, and Chong Zhang. Automatic labeling of vascular structures with topological constraints via HMM. 2017. doi: 10.5281/zenodo.809931. URL http://repositori.upf.edu/handle/10230/32744. Accepted: 2017-09-05T15:38:27Z Publisher: Springer.

Linlin Yao, Pengbo Jiang, Zhong Xue, Yiqiang Zhan, Dijia Wu, Lichi Zhang, Qian Wang, Feng Shi, and Dinggang Shen. Graph convolutional network based point cloud for head and neck vessel labeling. In Mingxia Liu, Chunfeng Lian, Pingkun Yan, and Xiaohuan Cao, editors, *Machine Learning in Medical Imaging - 11th International Workshop, MLMI 2020, Held in Conjunction with MICCAI 2020, Proceedings*, Lecture Notes in Computer Science (including subseries Lecture Notes in Artificial Intelligence and Lecture Notes in Bioinformatics), pages 474–483, Germany, 2020. Springer Science and Business Media Deutschland GmbH. ISBN 9783030598600. doi: 10.1007/978-3-030-59861-7_48. Publisher Copyright: © 2020, Springer Nature Switzerland AG.; 11th International Workshop on Machine Learning in Medical Imaging, MLMI 2020, held in conjunction with the 23rd International Conference on Medical Image Computing and Computer Assisted Intervention, MICCAI 2020 ; Conference date: 04-10-2020 Through 04-10-2020.